Vector-Resolved Magnetooptic Kerr Effect Measurements of Spin–Orbit Torque

Halise Celik[1], Harsha Kannan[1], Tao Wang[1], Alex R. Mellnik[2,3], Xin Fan[4], Xinran Zhou[5], Rasoul Barri[1], Daniel C. Ralph[2], Matthew F. Doty[5], Virginia O. Lorenz[6], and John Q. Xiao[1]

[1]Department of Physics and Astronomy, University of Delaware, Newark, DE 19716 USA
[2]Department of Physics, Kavli Institute at Cornell for Nanoscale Science, Cornell University, Ithaca, NY 14853 USA
[3]Intel Corporation, Hillsboro, OR 97124 USA
[4]Department of Physics and Astronomy, University of Denver, Denver, CO 80210 USA
[5]Department of Materials Science and Engineering, University of Delaware, Newark, DE 19716 USA
[6]Department of Physics, University of Illinois at Urbana–Champaign, Urbana, IL 61801 USA

We demonstrate simultaneous detection of current-driven dampinglike and fieldlike spin–orbit torques in heavy metal/ferromagnetic metal bilayers by measuring all three magnetization components m_x, m_y, and m_z using a vector-resolved magnetooptic Kerr effect (MOKE) technique based on quadrant detection. We investigate the magnitude and direction of spin–orbit torques in a series of platinum/permalloy samples, finding good agreement with results obtained via polar and quadratic MOKE measurements without quadrant detection.

Index Terms— **Magneto-optic effects, spintronics.**

I. Introduction

SPIN–ORBIT coupling-driven phenomena such as the spin Hall effect (SHE) [1] and Rashba effect [2] enable manipulation of magnetization via electric current. By using electric current to control the magnetization of nanoscale elements, it is possible to efficiently integrate magnetic functionalities into electronic circuits [3] and accelerate the technological development of high-performance and high-density magnetic storage devices [4]–[11].

In heavy metal (HM)/ferromagnetic metal (FM) bilayers, an electric current will generate dampinglike spin–orbit torque (DT) and fieldlike spin–orbit torque (FT), which will change the magnetization direction. In order to quantify the magnitude and the direction of magnetization reorientation due to DT and FT generated by the SHE and Rashba effects, electrical measurement techniques such as the anomalous Hall effect and second-harmonic Hall effect have been implemented for samples with perpendicular magnetic anisotropy [12]. The planar Hall effect has also been used for samples with in-plane anisotropy [13]. However, these methods are second-order measurements and are susceptible to thermal effects or rectification effects due to other nonlinear processes that are common in magnetic materials.

Previously, we have shown that normal incidence light can measure both current-induced out-of-plane magnetization reorientation by polar magnetooptic Kerr effect (MOKE) measurements [14] and in-plane magnetization reorientation by the second-order (quadratic) MOKE measurements [15] using a balanced detector. Such MOKE techniques do not suffer from electrical artifacts, and for high-sensitivity measurements, potential optical artifacts such as reflectivity changes can be separated from the MOKE signal harmonically [16].

In ferromagnetic thin films, there have been several studies to determine the magnetization components vectorially [17], [18]. For example, Ding *et al.* [19] proposed a method to distinguish the pure longitudinal and polar Kerr contributions via two separate measurements, interchanging the positions of a light source and a detector. Yang and Scheinfein [20] showed the detection of three magnetization components by changing the different relative orientations of the optical devices: polarizer, modulator, and analyzer. As an alternative that does not require changing the position of optical elements or data analysis to separate overlapping signals from different vector components, Keatley *et al.* [21] used a scanning Kerr microscope equipped with a compact optical quadrant bridge polarimeter to measure in-plane vector hysteresis loops.

II. Vector-Resolved MOKE Measurements

Here, we present vector-resolved MOKE measurements of spin–orbit torque based on an optical quadrant bridge detector for the first-order detection of current-induced DT and FT in HM/FM bilayers over a wide range of thicknesses. With this vector-resolved MOKE technique, where normal incidence is converted to various incident angles with the help of an objective lens, one can separate the MOKE effects that are linear and quadratic in the magnetization and determine all three components of the magnetization vector. Thus, we can measure both DT and FT components simultaneously without the need to measure quadratic MOKE. We apply this method to measure DT and FT for a series of platinum (Pt)/permalloy ($Ni_{81}Fe_{19}$ = Py) samples as a demonstration of the implementation of the proposed technique. We compare our results with

Manuscript received April 21, 2018; revised July 30, 2018; accepted September 18, 2018. Date of publication December 3, 2018; date of current version December 18, 2018. Corresponding author: J. Q. Xiao (e-mail: jqx@udel.edu).

Color versions of one or more of the figures in this paper are available online at http://ieeexplore.ieee.org.

Digital Object Identifier 10.1109/TMAG.2018.2873129

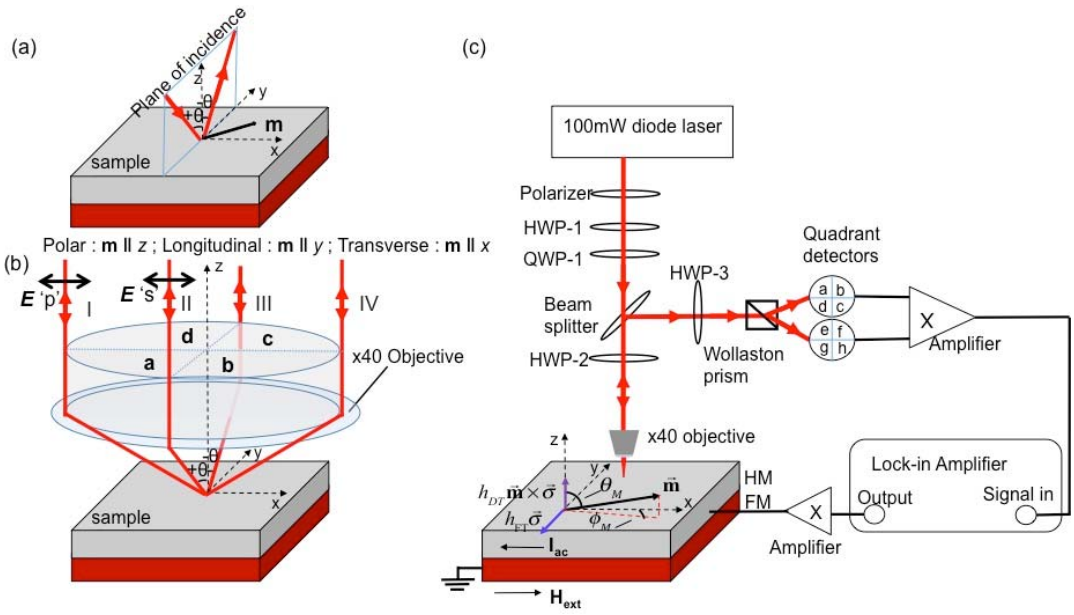

Fig. 1. (a) Polar, longitudinal, and transverse MOKE geometries for a sample with magnetization m. (b) Geometry of the optical quadrant bridge detection system. A 40× objective focusses light transmitted to and collimates light reflected from the sample. The reflected light is detected in spatial quadrants a, b, c, and d. By adding and subtracting signals from appropriate quadrants, one can isolate the in-plane MOKE response from the out-of-plane MOKE response. (c) Experimental setup for the optical detection of spin–orbit torques. HWP: half-wave plate. QWP: quarter-wave plate.

measurements made using polar and quadratic MOKE without quadrant detection.

The Landau–Lifshitz–Gilbert–Slonczewski equation is usually used to describe the DT and FT generated from a current through the HM/FM bilayer [22]

$$\frac{d\vec{M}}{dt} = -\gamma\,\vec{M}\times\vec{H} + \frac{\alpha}{M_s}\vec{M}\times\frac{d\vec{M}}{dt} + a\vec{M}\times\vec{\sigma} + b\vec{M}\times(\vec{\sigma}\times\vec{M}) \quad (1)$$

where σ is a unit vector for the spin direction that is in-plane and orthogonal to the electric current, a and b describe the FT and DT, respectively. The effective fields corresponding to the FT and DT can be defined as $\vec{h}_{\mathrm{FT}} = -a\vec{\sigma}/\gamma$ and $\vec{h}_{\mathrm{DT}} = -b\vec{\sigma}\times\vec{M}/\gamma$, respectively.

The magnetooptical properties of a material can be described by the permittivity tensor, ε_{ij}, which can be expanded in the components of the magnetization $\boldsymbol{m}$ acting on the material [23]: $\varepsilon_{ij} = \varepsilon_{ij}^{(0)} + K_{ijk}m_k + G_{ijkl}m_k m_l + \cdots$, where the Einstein summation convention over the x-, y-, and z-coordinates is used. The dielectric tensor $\varepsilon_{ij}^{(0)}$ represents the components of the permittivity tensor in the absence of magnetization m, K_{ijk} is the linear magnetooptic tensor, and G_{ijkl} is the quadratic magnetooptic tensor, which corresponds to a second-order MOKE response, often referred to as quadratic MOKE [24]. The linear response can be separated into terms corresponding to relative orientations of the unit vector of the magnetization $\hat{m}$, plane of incidence, and sample plane. By using appropriate polarization conditions, the transverse component is avoided. The Kerr rotation and ellipticity give a measure of the magnetization of the sample.

Since the Kerr effect exists for any arbitrary direction of the magnetization, for oblique incidence, the detected MOKE signal $\Psi(m)$ from a sample with magnetization $\boldsymbol{m}$ can be written as (assuming the transverse component is suppressed)

$$\Psi(m) = \alpha_{\mathrm{polar}}m_z + \gamma_{\mathrm{longitudinal}}m_y + \delta_{\mathrm{longitudinal}}m_x + \beta_{\mathrm{quadratic}}m_x m_y \cdots \quad (2)$$

where the z-direction is perpendicular to the magnetic film plane [see Fig. 1(a)], the y-direction is parallel to the plane of the incident polarization, and α_{polar}, $\gamma_{\mathrm{longitudinal}}$, $\delta_{\mathrm{longitudinal}}$, and $\beta_{\mathrm{quadratic}}$ are the coefficients for the polar, longitudinal, and quadratic MOKE responses, respectively.

It has been demonstrated that polar and longitudinal signals can be separated by measuring the Kerr signal in two reversed geometries [25], as the polar signal does not change sign if the angle of incidence is reversed from $+\theta$ to $-\theta$ but the longitudinal signal does change sign. That is, polar MOKE is an even function, whereas longitudinal MOKE is an odd function of the incident angle. Quadratic MOKE is also an even function of the incident angle, as shown in [26]. Thus, light incident at $-\theta$ [e.g., traveling from ray III to ray II in Fig. 1(b)] has the same sign for polar and quadratic signals but opposite sign for longitudinal signals as the light incident at $+\theta$ [e.g., traveling from ray II to ray III in Fig. 1(b)].

Using the even and odd dependence on the incident angle, we are able to separate polar, longitudinal, and quadratic MOKE responses. Using a microscope objective with a high numerical aperture (NA = 0.65 in our setup), we focus light across a wide range of incident angles from perpendicular to the sample plane to oblique (up to approximately 40°) [21]. The light reflected from the sample is measured in four quadrants, as shown in Fig. 1(b). By taking sums or differences of the four quadrants, we obtain the contributions from the polar, longitudinal, and quadratic responses, with the longitudinal contribution antisymmetric with incident angle. Thus, the response for angles of incidence θ with inward

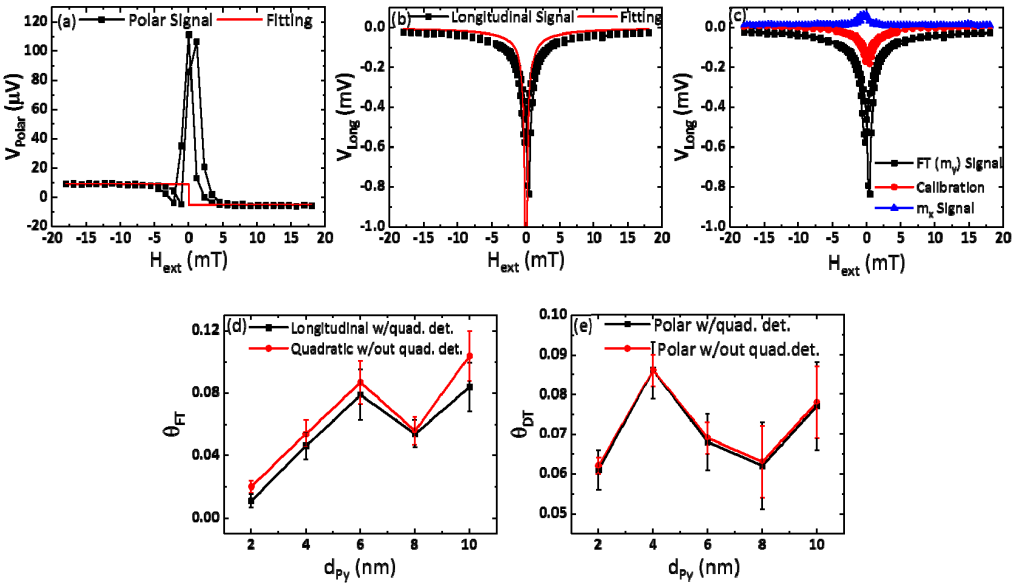

Fig. 2. (a) Current-induced polar and (b) longitudinal response as a function of the swept magnetic field H_{ext} in Py(8)/Pt(6) bilayers. The red lines are least-squares fits to a step function and to $\sim 1/H_{\text{ext}}$ for the polar and longitudinal responses, respectively. The difference between the polar signal and the fit near zero external field is due to the sample being in an unsaturated magnetization state at low field, which may result in domain formation. (c) Measured voltage from the lock-in amplifier as a function of the external magnetic field for Py(8)/Pt(6) when passing an ac current (20 mA) through the sample (black squares) and an ac current (500 mA) through a wire underneath the sample (red circles), signal in other longitudinal configuration, m_x (blue triangles). (d) Effective FT spin Hall angle measured via longitudinal with quadrant detection (black squares) and quadratic (red circles) MOKE versus permalloy thickness d_{Py}. (e) Effective DT spin Hall angle measured with polar MOKE with quadrant detection (black squares) and polar MOKE without quadrant detection (red circles) versus permalloy thickness d_{Py}.

$(+\theta)$ and outward $(-\theta)$ propagation can be represented as $\theta_{\text{K}}^{\pm\theta} = \theta_{\text{K}}^{P} \pm \theta_{\text{K}}^{L} + \theta_{\text{K}}^{Q}$, where $\theta_{\text{K}}^{\pm\theta}$ is the Kerr rotations for the respective angles of incidence, and $\theta_{\text{K}}^{P}, \theta_{\text{K}}^{L}$, and θ_{K}^{Q} are the rotations for the polar, longitudinal, and quadratic MOKEs, respectively. These terms contain the degree of polarization rotation measured via the balanced detection scheme shown in Fig. 1(c). On the detection arm, the quadrant detector allows us to either sum or subtract the inward $(\theta_{\text{K}}^{+\theta})$ and outward $(\theta_{\text{K}}^{-\theta})$ signals to obtain the desired Kerr rotations. By taking the sum of both inward $(\theta_{\text{K}}^{+\theta})$ and outward $(\theta_{\text{K}}^{-\theta})$ signals, one obtains twice the sum of the polar and quadratic Kerr rotations. Since we add the signals from two halves together, which corresponds to the signal measured at normal incidence, this signal does not have contributions from longitudinal or transverse MOKE. Polar MOKE response can be distinguished from the quadratic MOKE response by tuning the angle of polarization of the light. The polar MOKE response does not depend on the polarization direction, while the quadratic MOKE depends on the polarization angle ϕ_{pol} as $\cos 2\phi_{\text{pol}}$. Measurement at 45° polarization can be performed to cancel the quadratic contribution, which enables us to determine the polar contribution, and in turn the DT term. Details of the methodology for separating polar and quadratic responses can be found in our previous work [15]. By taking the difference of both inward $(\theta_{\text{K}}^{+\theta}$ = ray II) and outward $(\theta_{\text{K}}^{-\theta}$ = ray III) signals, one obtains twice the longitudinal Kerr rotation. This allows determination of one in-plane magnetization component m_y. For the longitudinal measurements, the incident light is p-polarized, but we take the difference of signals related to ray II and ray III in Fig. 1(b), which corresponds to s-polarized light; thus, no transverse MOKE signal is measured. The other in-plane magnetization component, m_x, can be gathered by subtracting the right (ray I) and the left (ray IV) halves of the beam. To suppress the transverse component for rays I and IV, the incoming polarization is changed from p-polarization to s-polarization. The Kerr rotation from the FT term and other in-plane longitudinal component can be measured in this way. In principle, a magnetization term proportional to $m_x m_z$ may generate a hysteresislike signal in the longitudinal configuration due to the out-of-plane Oersted field, but this term is anticipated to be less than two orders of magnitude smaller than the first-order signal, and the measured signals do not indicate any substantial contribution from this term.

III. Experimental Setup

A diagram of our vector-resolved MOKE setup is shown in Fig. 1(c). Collimated light from a 100 mW diode laser at 785 nm center wavelength goes through a Glan Taylor polarizer with an extinction coefficient of $\sim 10^{-4}$ to set the polarization. The angle of polarization is controlled with a half-wave plate (HWP-2) before being focused by a microscope objective of NA 0.65 on the sample. The reflected beam passes back through the objective and HWP-2 and is reflected by a 90/10 beam splitter. It goes through another HWP-3 and the vertical and horizontal polarization components are split by a Wollaston prism. The intensity of the two components is balanced by adjusting HWP-3. The polarization components are detected by two quadrant photodiode detectors whose outputs are the sums or differences of various halves of the beams. The outputs of the detectors are subtracted from each other to achieve common mode rejection and doubling of the

signal and then amplified. The signal is measured by a lock-in amplifier locked to the frequency of the ac current driving the sample. We have used the same set of samples we used in [15], namely, in-plane magnetized substrate/Pt(6 nm)/Py (d_{Py}) bilayers, with d_{Py} ranging from 2 to 10 nm to verify the accuracy of this method by comparing results found by two different methods.

We apply an in-plane ac current, $I_{\mathrm{ac}} \cos \omega t$, at 1733 Hz with $I_{\mathrm{ac}} = 20$ mA along the x-axis to the sample. An external magnetic field H_{ext} is applied along the x-axis to align the magnetization. The current-induced FT and DT rotate the magnetization within the sample plane (changing ϕ_{M}) and perpendicular to the plane (changing θ_{M}), respectively. The magnetization change due to current-induced torques for in-plane magnetized samples can be written in terms of two orthogonal effective magnetic field components h_{FT} and h_{DT}

$$\begin{cases} \Delta\phi_{\mathrm{M}} = \dfrac{h_{\mathrm{FT}}}{H_{\mathrm{ext}} + H_{\mathrm{a}\parallel}} \\ \Delta\theta_{\mathrm{M}} = \dfrac{h_{\mathrm{DT}}}{H_{\mathrm{ext}} + H_{\mathrm{a}\parallel} + M_{\mathrm{s}} - H_{\mathrm{a}\perp}} \end{cases} \tag{3}$$

where $H_{\mathrm{a}\parallel}$ is the in-plane anisotropy field, $H_{\mathrm{a}\perp}$ is the out of-plane anisotropy field, and M_{s} is the saturation magnetization. For an ordinary transition-metal ferromagnet such as permalloy, the in-plane anisotropy is negligible and M_{s} is much larger than any of the fields discussed here. Thus, for current-induced magnetization reorientation, the change in the polar MOKE signal (proportional to $\Delta\theta_{\mathrm{M}}$) should be approximately independent of the applied field for $H_{\mathrm{ext}} \ll M_{\mathrm{s}}$, while the current-induced change in the longitudinal MOKE signal (proportional to $\Delta\phi_{\mathrm{M}}$) should scale approximately as $1/H_{\mathrm{ext}}$. Examples of experimental results from 50 μm $\times$ 50 μm Py(8)/Pt(6), where the numbers in parentheses are thicknesses in nanometers, with a 20 mA bias current and 1 mW laser power are shown in Fig. 2(a) and (b). The current-induced spin–orbit torque signals obtained by the MOKE measurements exhibit the expected linear dependence on the applied current density [14].

Fig. 2(a) shows the raw data for the Py(8)/Pt(6) polar term (m_z) obtained using light at 45° polarization and taking the sum of all quadrants. It switches sign as the magnetization switches and is independent of H_{ext} away from zero field. Fig. 2(b) shows the longitudinal term (m_y) at 0° polarization (at which polarization, the transverse component is suppressed) exhibits a $1/H_{\mathrm{ext}}$ dependence.

The magnitude of the DT is determined through a self-calibration method explained in our previous publication [14]. Using a simple parallel circuit model to account for the different resistivities of Pt and Py, we estimate that approximately 42% of the current flows through the Pt, yielding a current density in Pt of $j_{\mathrm{Pt}} = 2.8 \times 10^{10} \mathrm{A/m}^2$. Note that the parallel circuit model does not take into account the potential for nonuniform conductance and thus may lead to overestimation of the current in the nonmagnetic layer [27]. A line scan is performed by keeping the laser position fixed and translating the sample along the y-direction. Fig. 3 shows a line scan obtained using quadrant detectors for Py(4)/Pt(6). The difference between lock-in voltages at positive saturation field and negative saturation field are taken for the DT signal and the summation of the lock-in voltages at positive saturation field and negative saturation field are taken for the out-of-plane Oersted field for each position. By fitting the lines' scans using quadrant detectors for the DT signal and out-of-plane Oersted field, we extract the DT coefficient $\beta_{\mathrm{T}} = (h_{\mathrm{DT}}/j_{\mathrm{Pt}}) = 6.970 \pm 0.050$ nm. The effective spin Hall angle is defined as the ratio of the out-of-plane spin current to the in-plane charge current and is given by $\theta_{\mathrm{SH}} = \beta_{\mathrm{T}}((2e/\hbar))\mu_0 M_{\mathrm{s}} d_{\mathrm{Py}}$. Since the spin–orbit torques consist of two components: DT and FT, two spin Hall torque efficiencies are calculated. Assuming that the DT arises from the SHE and using the equation $\theta_{\mathrm{SH}} = \beta_{\mathrm{T}}((2e/\hbar))\mu_0 M_{\mathrm{s}} d_{\mathrm{Py}}$, we determine an effective spin Hall angle for DT, $\theta_{\mathrm{DT}} = 0.086 \pm 0.007$ from vector-resolved MOKE for Pt, which is the same as that obtained with polar and quadratic MOKE without quadrant detection $\theta_{\mathrm{DT}} = 0.086 \pm 0.004$, [15]. Here, the parameters used are $\mu_0 M_{\mathrm{s}} d_{\mathrm{Py}} = 4.080$ T $\cdot$ nm.

To determine the magnitude of the FT, we perform a calibration by passing an ac current (500 mA) only through a metallic wire (1 mm wide and 1 cm long) behind the sample that drives in-plane magnetization reorientation due to Ampere's law. Since this current is not passing through the sample, it does not contribute to spin–orbit torques. This ac current generates an Oersted field of 70.700 $\pm$ 2.940 A/m. The distance from the sample to the wire is about 1.050 $\pm$ 0.050 mm.

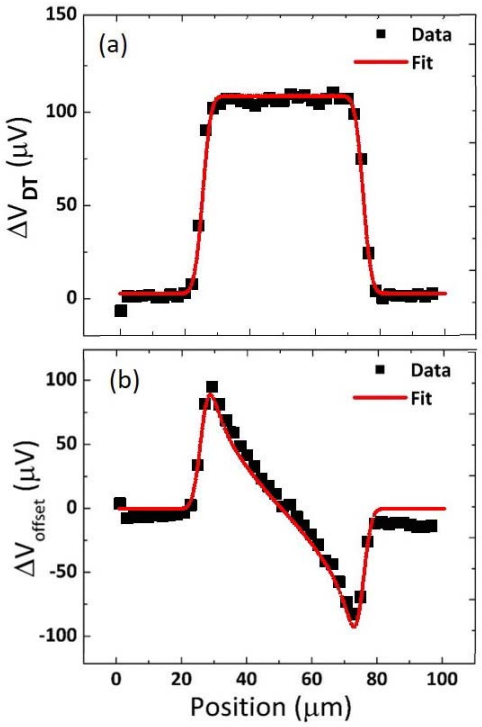

Fig. 3. (a) Line scan result for Py(4)/Pt(6) with quadrant detectors. DT field detected by subtracting signals taken at positive and negative saturation field. Fit function (red line) is calculated as the integration of the DT-induced magnetization reorientation weighted by the Gaussian function that describes the spatial distribution of the laser. (b) Out-of-plane Oersted field detected by addition of signals taken at positive and negative saturation field. The fit function for the Oersted field (red line) is similarly calculated as the integration of the local magnetization reorientation weighted by the Gaussian function that describes the spatial distribution of the laser.

The magnitude of the FT is extracted using a linear regression algorithm by comparing the FT signal curve and the calibration curve shown in Fig. 2(c) for Py(8)/Pt(6). In this example fitting, the ratio between the signals corresponding to the current-induced effective field and the calibration field is 2.490 ± 0.070, which corresponds to a current-induced field of 176.080 ± 5.310 A/m. After removing the 83.800 A/m Oersted field generated by the current in the sample, we obtain $h_{\mathrm{FT}} = 92.280 \pm 5.310$ A/m, which gives an effective spin Hall angle of $\theta_{\mathrm{FT}} = 0.054 \pm 0.003$. We also measure the change in the other in-plane magnetization component m_x, which is negligibly small as expected.

To further verify the accuracy of this method, we have extracted the effective spin Hall angle from FT and DT measurements for permalloy thicknesses d_{Py} from 2 to 10 nm and compared the results with quadratic MOKE and polar MOKE obtained without quadrant detection, respectively. As shown in Fig. 2(d) and (e), the spin Hall angles determined from the longitudinal and polar measurements with quadrant detection agree well with the angles determined from quadratic and polar MOKE measurements without quadrant detection, respectively. The precision of the quadrant detection technique is similar to that achieved via quadratic MOKE without quadrant detection. Thus, the quadrant detection method provides an alternative technique that can be chosen based on the experimenter's available equipment, preference for first-order response versus second-order response, and analysis methods.

IV. Conclusion

In conclusion, we have demonstrated a convenient vector-resolved MOKE technique that can simultaneously measure the current-induced dampinglike and fieldlike torques using normally-incident light. We find quantitative agreement between the results of this technique and quadratic and polar MOKE measurements done without quadrant detection for a series of Pt/Py bilayers with different Py thicknesses. The technique can be easily extended to measure spin–orbit torques in systems with perpendicular magnetization, as well as in systems with arbitrary magnetization direction. We anticipate this technique will be useful for further studies of current-induced magnetization reorientation in a variety of materials.

Acknowledgment

This work was supported in part by the Department of Energy under Grant DE-SC0016380 and in part by the National Science Foundation under Grant DMR-1624976.

References

[1] M. I. Dyakonov and V. I. Perel, "Current-induced spin orientation of electrons in semiconductors," *Phys. Lett. A*, vol. 35, no. 6, pp. 459–460, 1971.

[2] E. I. Rashba, "Symmetry of energy bands in crystals of wurtzite type. 1. Symmetry of bands disregarding spin-orbit interaction," *Sov. Phys. Solid State*, vol. 1, no. 3, pp. 368–380, 1959.

[3] Y. Li *et al.*, "Anisotropic current-controlled magnetization reversal in the ferromagnetic semiconductor (Ga,Mn)As," *Appl. Phys. Lett.*, vol. 103, no. 2, p. 022401, 2013.

[4] E. B. Myers, D. C. Ralph, J. A. Katine, R. N. Louie, and R. A. Buhrman, "Current-induced switching of domains in magnetic multilayer devices," *Science*, vol. 285, no. 5429, pp. 867–870, 1999.

[5] M. Weisheit, S. Fähler, A. Marty, Y. Souche, C. Poinsignon, and D. Givord, "Electric field-induced modification of magnetism in thin-film ferromagnets," *Science*, vol. 315, no. 5810, pp. 349–351, 2007.

[6] Y.-H. Chu *et al.*, "Electric-field control of local ferromagnetism using a magnetoelectric multiferroic," *Nature Mater.*, vol. 7, pp. 478–482, Apr. 2008.

[7] T. Maruyama *et al.*, "Large voltage-induced magnetic anisotropy change in a few atomic layers of iron," *Nature Nanotechnol.*, vol. 4, pp. 158–161, Jan. 2009.

[8] I. M. Miron *et al.*, "Perpendicular switching of a single ferromagnetic layer induced by in-plane current injection," *Nature*, vol. 476, pp. 189–193, Aug. 2011.

[9] L. Liu, C.-F. Pai, Y. Li, H. W. Tseng, D. C. Ralph, and R. A. Buhrman, "Spin-torque switching with the giant spin Hall effect of tantalum," *Science*, vol. 336, no. 6081, pp. 555–558, 2012.

[10] S. Emori, U. Bauer, S.-M. Ahn, E. Martinez, and G. S. D. Beach, "Current-driven dynamics of chiral ferromagnetic domain walls," *Nature Mater.*, vol. 12, pp. 611–616, Jun. 2013.

[11] K.-S. Ryu, L. Thomas, S.-H. Yang, and S. Parkin, "Chiral spin torque at magnetic domain walls," *Nature Nanotechnol.*, vol. 8, pp. 527–533, Jun. 2013.

[12] K. Garello *et al.*, "Symmetry and magnitude of spin–orbit torques in ferromagnetic heterostructures," *Nature Nanotechnol.*, vol. 8, pp. 587–593, Jul. 2013.

[13] X. Fan, J. Wu, Y. Chen, M. J. Jerry, H. Zhang, and J. Q. Xiao, "Observation of the nonlocal spin-orbital effective field," *Nature Commun.*, vol. 4, Apr. 2013, Art. no. 1799.

[14] X. Fan *et al.*, "Quantifying interface and bulk contributions to spin–orbit torque in magnetic bilayers," *Nature Commun.*, vol. 5, Jan. 2014, Art. no. 3042.

[15] X. Fan *et al.*, "All-optical vector measurement of spin-orbit-induced torques using both polar and quadratic magneto-optic Kerr effects," *Appl. Phys. Lett.*, vol. 109, no. 12, p. 122406, 2016.

[16] C. Stamm *et al.*, "Magneto-optical detection of the spin Hall effect in Pt and W thin films," *Phys. Rev. Lett.*, vol. 119, no. 8, p. 87203, 2017.

[17] A. Berger and M. R. Pufall, "Quantitative vector magnetometry using generalized magneto-optical ellipsometry," *J. Appl. Phys.*, vol. 85, no. 8, p. 4583, 1999.

[18] T. Kuschel *et al.*, "Vectorial magnetometry using magnetooptic Kerr effect including first- and second-order contributions for thin ferromagnetic films," *J. Phys. D, Appl. Phys.*, vol. 44, no. 26, p. 265003, 2011.

[19] H. F. Ding, S. Pütter, H. P. Oepen, and J. Kirschner, "Spin-reorientation transition in thin films studied by the component-resolved Kerr effect," *Phys. Rev. B, Condens. Matter*, vol. 63, no. 13, p. 134425, 2001.

[20] Z. J. Yang and M. R. Scheinfein, "Combined three-axis surface magneto-optical Kerr effects in the study of surface and ultrathin-film magnetism," *J. Appl. Phys.*, vol. 74, no. 11, p. 6810, 1993.

[21] P. S. Keatley *et al.*, "Time-resolved investigation of magnetization dynamics of arrays of nonellipsoidal nanomagnets with nonuniform ground states," *Phys. Rev. B, Condens. Matter*, vol. 78, no. 21, p. 214412, 2008.

[22] J. C. Slonczewski, "Currents and torques in metallic magnetic multilayers," *J. Magn. Magn. Mater.*, vol. 247, no. 3, pp. 324–338, 2002.

[23] J. Hamrlová, J. Hamrle, K. Postava, and J. Pištora, "Quadratic-in-magnetization permittivity and conductivity tensor in cubic crystals," *Phys. Status Solidi Basic Res.*, vol. 250, no. 10, pp. 2194–2205, 2013.

[24] M. Buchmeier, R. Schreiber, D. E. Bürgler, and C. M. Schneider, "Thickness dependence of linear and quadratic magneto-optical Kerr effects in ultrathin Fe(001) films," *Phys. Rev. B, Condens. Matter*, vol. 79, no. 6, p. 064402, 2009.

[25] H. F. Ding, S. Pütter, H. Oepen, and J. Kirschner, "Experimental method for separating longitudinal and polar Kerr signals," *J. Magn. Magn. Mater.*, vol. 212, nos. 1–2, pp. 5–11, 2000.

[26] J. Hamrle *et al.*, "Huge quadratic magneto-optical Kerr effect and magnetization reversal in the Co_2FeSi Heusler compound," *J. Phys. D, Appl. Phys.*, vol. 40, no. 6, p. 1563, 2007.

[27] K. Chen and S. Zhang, "Roles of nonlocal conductivity on spin Hall angle measurement," *Phys. Rev. B, Condens. Matter*, vol. 96, no. 13, p. 134401, 2017.